Available online at www.sciencedirect.com
ScienceDirect
Polymer 48 (2007) 6448–6456
polymer
www.elsevier.com/locate/polymer

A molecular dynamics study of short-chain ordering in crystalline $LiPF_6 \cdot PEO_6$

A. Liivat [a], D. Brandell [a,*], A. Aabloo [b], J.O. Thomas [a]

[a] *Department of Materials Chemistry, Ångström Laboratory, Uppsala University, Box 538, SE-751 21 Uppsala, Sweden*
[b] *Institute of Technology, Tartu University, Nooruse 1, 50411 Tartu, Estonia*

Received 26 June 2007; received in revised form 14 August 2007; accepted 14 August 2007
Available online 24 August 2007

Abstract

Molecular dynamics (MD) simulations have been made of the crystalline short-chain $LiPF_6 \cdot PEO_6$ system to probe structural ordering for different chain-end arrangements for a methyl-terminated monodisperse poly(ethylene oxide) (EO_{23} $M_w = 1059$) host polymer. Five different start structures have been studied, two ''smectic'' and three ''nematic'', to represent different types of relative alignment of the end-groups between adjacent PEO chains, and different chain-end coordination situations to the Li-ions. One particular situation is found to result effectively in Li-ion bridging between PEO chains along the chain axes, thereby creating continuous ion transport pathways across the chain breaks. This situation is also found to give rise to $Li^+-PF_6^-$ ion-pairing and Li–O coordination instabilities in the end-group regions, where coordination to Li-ions would appear to have a more radical influence on local structure than the issue of *smectic vs. nematic* end-group alignment. It could be that such structural situations involving bridging Li-ions (in both *smectic* and *nematic* arrangements) are a necessary condition for the promotion of Li-ion transport in the chain direction. Comparison of simulated and experimental XRD profiles is concluded to be an inappropriately crude and uncertain technique for distinguishing between possible short-chain ordering models.

Keywords: Polymer electrolytes; End-group ordering; $LiPF_6 \cdot PEO_6$

1. Introduction

Poly(ethylene oxide)-based solid polymer electrolytes have been studied considerably for 30 years as promising materials for all-solid-state rechargeable Li-ion batteries [1,2]. By the mid 1980s, it had become widely accepted that only amorphous phases of PEO-based electrolytes conduct ions. Much of the research since then has therefore focused on suppressing crystallinity in PEO–salt complexes below their glass-transition temperature around 60 °C.

More recently, however, the discovery of new crystalline phases of $LiXF_6 \cdot PEO_6$ (X = P, As or Sb) [3,4] with higher conductivity than their amorphous counterparts have challenged this conventional wisdom, and raised questions as to the ionic conductivity mechanisms in these materials [5]. An increase by more that an order of magnitude in the rather low conductivity ($<10^{-7}$ S cm^{-1}) at ambient temperatures has also been reported through doping with aliovalent SiF_6^{2-} anions [6]. This effect has been modelled in our earlier work [7]. We can note that the structures of these compounds differ distinctly from other crystalline PEO–salt complexes in that they involve complete structural dissociation of the ionic species. The Li-ions are confined to lie along the tunnels formed by two PEO hemi-helices (Fig. 1). NMR data has suggested a Li^+-dominated ion transport [8]. This has been challenged in our subsequent molecular dynamics (MD) simulation study [7].

Unfortunately, the structural model resulting from the refinement of Neutron Diffraction (ND) data for long-chain PEO ($M_w = 28\,400$) [4] – the basis of our original infinite-chain MD model [9] – contains no information about local

* Corresponding author. Present address: Macromolecular and Interfaces Institute, Chemistry Department, Virginia Tech, Blacksburg, VA 24061, USA.
E-mail address: brandell@vt.edu (D. Brandell).

0032-3861/$ - see front matter © 2007 Elsevier Ltd. All rights reserved.
doi:10.1016/j.polymer.2007.08.051

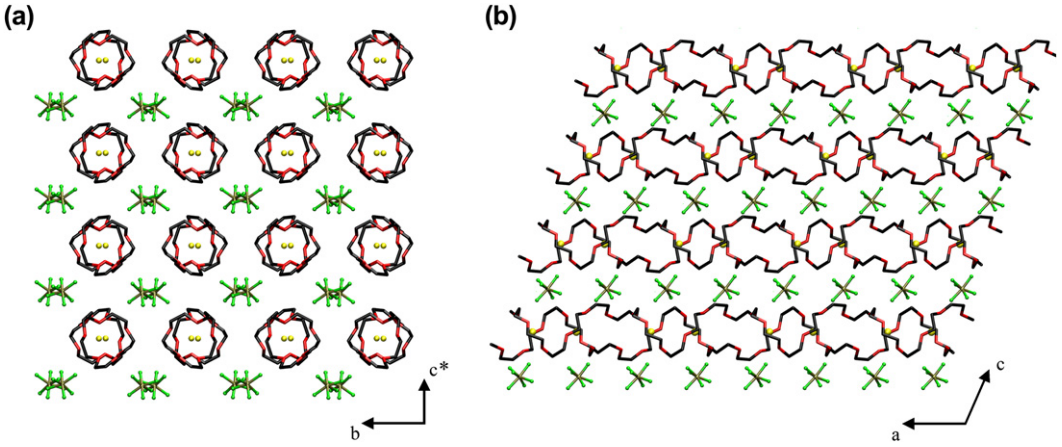

Fig. 1. The structure of crystalline $LiPF_6 \cdot PEO_6$; (a) view along the polymer channel axis, showing the Li-ions inside the channels and the PF_6^- outside; (b) view along the unique monoclinic axis (only top layer shown for clarity), showing the cation and anion positions and chain configuration.

defects such as chain-ends, site vacancies and crystallite interfaces. It is precisely these defects which can determine the prevalence of anion or cation transport. In the absence of experimental structural data, it is therefore important to understand the role of these chain-end defect regions.

The observed increase in ionic conductivity on decreasing the PEO chain-length in crystalline phases of $LiPF_6 \cdot PEO_6$ has previously been attributed to the increase in crystallite size [8], thereby facilitating longer pathways for ion transport and lower grain-boundary resistance. However, the quantitative experimental evidence to support this increase in crystallite size (from 200 to 250 nm) on decreasing the M_w of the PEO chains from 2000 to 1000 was based on peak shape analysis of a single non-overlapping XRD peak – the (0 2 1) reflection. Since this reflection is insensitive to crystallite size along the *a*-axis, which is the direction of the PEO channels (see Fig. 1), the calculated increase in crystallite size applies to the directions perpendicular to the PEO channels. This fact encourages us to consider models of PEO chain arrangements which support pathways for ion transport in these alternative directions.

We have earlier performed MD simulations for *smectic* and *nematic* arrangements of PEO chain-ends, as representing extremes of order and disorder in the spatial distributions of the methoxy end-groups [10]. In a recent paper [11], Bruce et al. specifically address these models when interpreting XRD and impedance spectroscopy data for crystalline systems containing poly- and monodisperse methoxy-capped ($M_w \sim 1000$) PEO chains. They attribute the lower observed ionic conductivity in the monodisperse system to a more ordered distribution of end-groups [11]; such order is clearly unfeasible in polydisperse systems. It has therefore now become highly relevant to consider the effect of increasing the concentration of chain-end defects as we go to shorter-chain PEO–salt systems. In this study, we extend our earlier MD simulations of the short-chain polymer–salt system $LiPF_6 \cdot PEO_6$ [9] to probe a variety of spatial arrangements of polymer end-groups in $LiPF_6 \cdot PEO_6$ crystals for the case of short-chain monodisperse PEO ($M_w = 1059$).

2. MD methods and models

The molecular dynamics (MD) simulation technique involves the routine integration of classical Newton's equations of motion of a many-atom system. If this is done sequentially at sufficiently short time intervals, the procedure should result in a complete history of atomic trajectories over a limited time period. The interatomic forces are described by simple analytical functions (the force-field) involving parameters evaluated empirically or from quantum mechanical calculations. This methodology has been well established for PEO-based polymer electrolytes [12,13].

The simulation details here are generally the same as in our earlier work [7,9,10]. All inter- and intramolecular force-field parameters for PEO were taken from Neyertz et al. [12], except for the bond-stretching and methyl-group rotation potentials; these are adapted from Jaffe et al. [14] and Borodin and Smith [15]. The parameters for the interaction of PEO, Li^+ and PF_6^- are taken from [16,17]. Simulations were run using the DL_POLY [18] program at 293 K, employing a Nosé–Hoover thermostat with temperature relaxation time of 0.1 ps. A constant volume ensemble (NVT) was used for 1 ns, followed by a constant anisotropic pressure (NσT) simulation for 1 ns, with a corresponding relaxation time 0.3 ps. Trajectory data were sampled at 0.1 ps intervals for subsequent analysis.

The start structures in the MD simulation boxes comprised $4 \times 2 \times 4$ unit cells of crystalline $LiPF_6 \cdot PEO_6$ [4] (see Fig. 1), with dimensions: $a = 46.928$ Å, $b = 34.750$ Å, $c = 34.768$ Å, $\beta = 107.8°$, involving 32 PEO hemi-helices of CH_3–$(OCH_2$-$CH_2)_{23}$–OCH_3, along with 128 $LiPF_6$ units. Terminal methyl groups were incorporated by breaking a C–C bond in the chain and attaching an extra hydrogen atom to each end-carbon, with H–C–H angles constrained to 109.45° and C–H distances to 1.1 Å. Both CH_3-groups were constrained to preserve (C_{3v}) symmetry, and rotated both about the C–O and O–C_{meth} bonds using a Monte-Carlo procedure to arrive at an orientation free from steric hindrance.

As in our earlier simulations, it was found that Li-ion jump events were virtually non-existent in the absence of an

imposed electric field. To learn anything about the structural conditions which relate to ion mobility, it was necessary to create a range of models to represent different structural situations we might reasonably expect to encounter in this type of system. A related approach has been used by Vouyovitch et al. to try to predict the 3D structure of a novel polythiophene, where no crystallographic structure determination was possible [19]. In total, five models were simulated: two *smectic* and three *nematic*; see models **1**–**5** in Fig. 2:

Smectic-A (**1** in Fig. 2): the chain-ends here are all arranged in planes to form a common interface, with the Li-ions all 6-fold coordinated to ether oxygens within the same PEO double hemi-helix (three from each); see also the upper figures in Fig. 2.

Smectic-B (**2** in Fig. 2): same as *Smectic-A* except that Li-ions bridge the interface and are coordinated to PEO chains on both sides of the *smectic* plane. In this way, we introduce a disorder feature into the Li-ion coordination at the interface. Again, see the upper figures in Fig. 2.

Nematic-A and *Nematic-B* (**3** and **4** in Fig. 2): these models are derived from their corresponding *smectic* counterparts through random displacement of neighbouring hemi-helical PEO pairs along the channel direction. These types of configuration were suggested by Bruce et al. to best represent the crystal structure for monodisperse systems [11].

Nematic-R (**5** in Fig. 2): this is the most disordered of the models simulated in which all chain-breaks occur randomly throughout the structure. This model corresponds to that proposed in Ref. [11] as the most rational structure for polydisperse systems.

Within this *smectic*/*nematic* classification of start structures, we also distinguish two types of chain-end coordination around the Li-ions: *ideal* coordination, in which chain termination does not disrupt either of the polymer chains involved in the 6-fold coordination sphere of a Li-ion, and *broken*-coordination, where this is not the case. *Smectic-A*, and *Nematic-A* thus involve *ideal* coordination, while *Smectic-B* and *Nematic-B* contain *broken*-coordination. *Nematic-R* involves both types of coordination, but the majority are broken.

This issue of order/disorder in Li-ion coordination has largely been overlooked earlier because the crystalline oligoether–salt complexes studied have involved either very short monodisperse PEO oligomers [20–23], where the coordination in stoichiometric complexes is well defined, or much longer polydisperse chains, where the lower concentration of chain-ends renders them of minor significance. However,

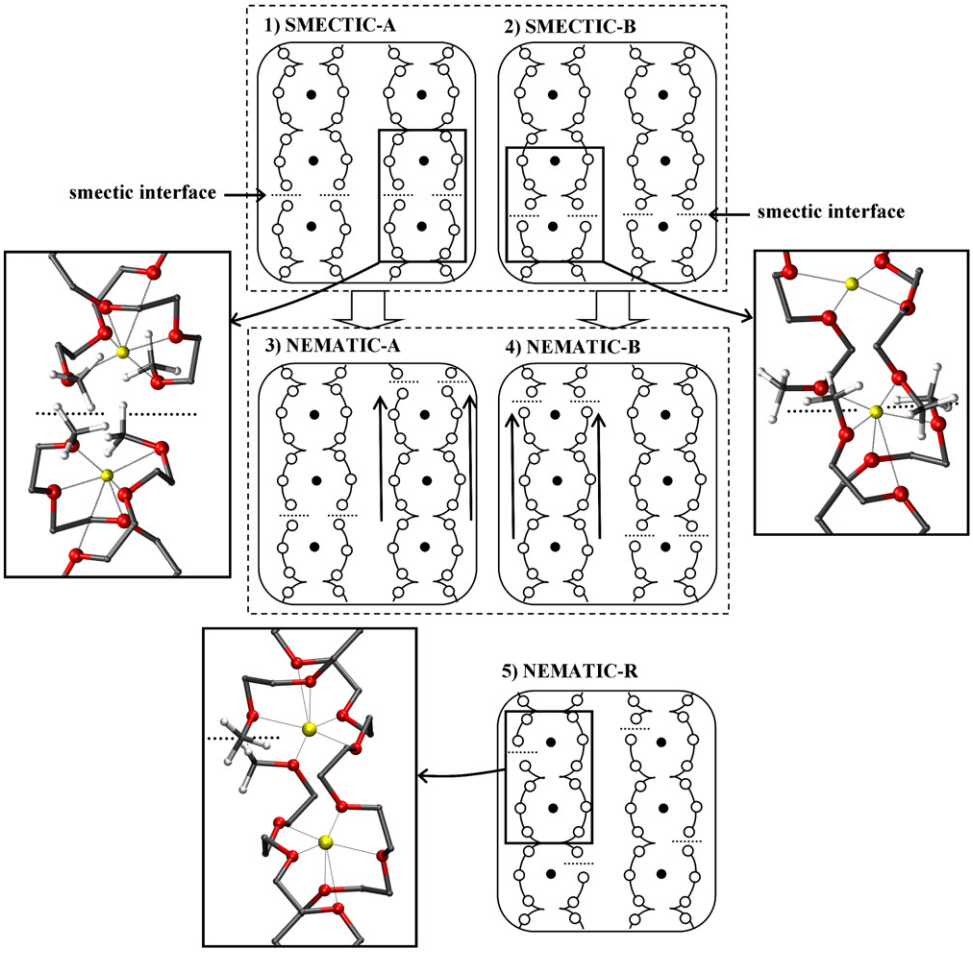

Fig. 2. A schematic representation of the models simulated for $LiPF_6 \cdot PEO_6$; (1) *Smectic-A* with the chain-breaks outside the 6-fold Li–O coordination sphere; (2) *Smectic-B* with the chain-breaks perturbing the 6-fold Li–O coordination; (3) and (4) *Nematic-A* and *Nematic-B*, derived from the corresponding *smectic* models by shifting adjacent PEO channels along their axes (see arrows); (5) *Nematic-R* has randomised chain-break locations. Typical snapshots of structural detail within chain-break regions are given at the top of the figure.

a study of single crystals of PEO_3(MW ~ 500)$LiCF_3SO_3$ has revealed a high selectivity to polymer chain-lengths on crystal formation [24]. Chain ordering is therefore analysed in terms of two distinct structural features: (i) ordering of neighbouring chain-ends; and (ii) the coordination (ideal or broken) of Li-ions to the polymer chain, since short-chain ordering has been proposed to be a significant factor in determining ion transport mechanisms in these materials [11].

3. Results and discussion

Visual inspection of sampled snapshots could readily confirm that all the simulated systems maintained the general characteristics of their start structures – with cylindrical double hemihelical PEO channels still separating the Li-ions within the channels from the PF_6^- anions outside the channels. All structural disruptions are located in the vicinity of the end-groups. A modest incidence of ion-pairing is also noted in the systems involving broken Li-ion coordination in the defect regions.

Another observation is that the shape and size of all MD boxes are generally retained for all models when their geometry is released on going from NVT to NσT ensemble simulation. Interestingly, all boxes tend to shift in the same general way: the *a*-axes (the polymer chain direct) all expand (on average by 2.5%), which could reflect that the attractive forces between chain-ends are too weak, while the *b*- and *c*-axes both contract by roughly the same amount (on average by 2.6 and 2.7%, respectively), indicating that the attractive forces between the polymer chains are too strong.

It is clearly not meaningful to attempt to extract any more detailed information than this from these observed discrepancies; the relationship between the NσT MD box shape/size and individual structural feature is so complex.

3.1. Li–O coordination and ion-pairing

The models involving ideal 6-fold Li–O coordination all maintain this coordination number (CN) throughout the simulations, even in defect regions (see Fig. 3; *Smectic-A* and *Nematic-A*), while CN(Li–O) is seen to vary from 4 to 7 in the remainder of the systems simulated. Such variations in broken-coordination situations occur mainly in defect regions involving 2–3 Li-ions (Fig. 4). The 7-fold Li–O coordination (dashed line in Fig. 4) is unstable, with the 7th coordinating oxygen spending typically <5 ps at a Li–O distance less than 3 Å. A typical *Smectic-B* broken-coordination situation is demonstrated in Fig. 5: in the left-hand channel, the Li-ion on the lower side of the defect region remains coordinated

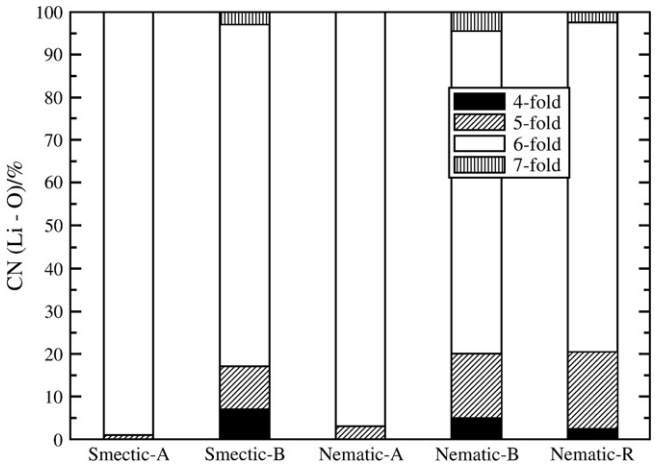

Fig. 3. Distribution of Li coordination numbers CN(Li–O) for the five simulated $LiPF_6 \cdot PEO_6$ systems (see Fig. 2).

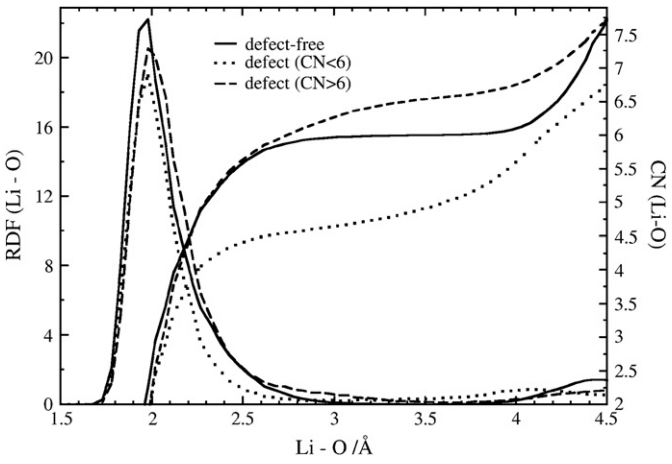

Fig. 4. Li–O radial distribution functions RDF(Li–O) and coordination numbers CN(Li–O) for the *Nematic-B* $LiPF_6 \cdot PEO_6$ model with defect-free and defect regions plotted separately.

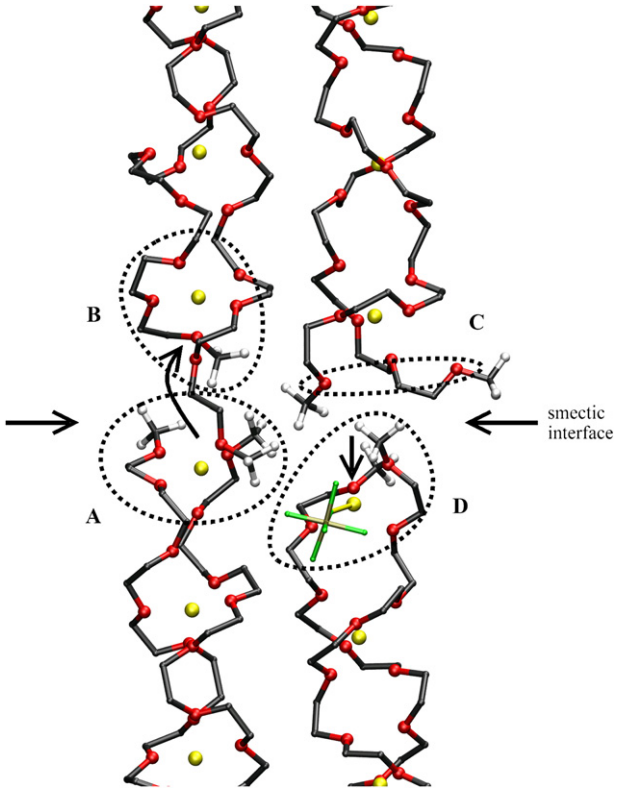

Fig. 5. PEO chain conformation rearrangements and corresponding Li coordination in the defect region of the *Smectic-B* model of $LiPF_6 \cdot PEO_6$.

by one end-group oxygen belonging to the next polymer chain (**A**), whereas another oxygen has migrated to coordinate to the Li-ion on the upper side of the defect (**B**). In the right-hand channel, however, both chain-ends from the polymer channel at the upper end of the defect have left the coordination sphere of the Li-ion on the lower side of the defect, resulting in two uncoordinated methoxy groups in the defect region (**C**). This deficit of coordinating oxygens around the Li-ion on the lower side of the gap causes this channel end-region to contract, thus allowing ion-pair formation (**D**). The persistence of the ''Li-bridging'' coordination (**A**) shown in Fig. 5 can have an important impact on the overall stability of the structure.

Ion-pairing thus occurs predominantly in coordination situations which involve exclusively Li-ions with low CN(Li–O); see Fig. 6a. Through competition with the coordinating ether oxygens, Li–F coordination is always 1-fold, unless the Li-ion has migrated outside the PEO channel. Since defect regions contain uncoordinated methoxy groups (Fig. 5 **C**), ion pairs occasionally dissociate, thereby restoring the bridging configuration **A** shown in Fig. 5. These ion association–dissociation events occur on a nanosecond time-scale and correlate with changes in CN(Li–O); pair formation leads to a decrease in CN(Li–O) and *vice versa*.

The proportion of Li-ions with 4-fold coordination decreases in the systems simulated in the order: *Smectic-B* > *Nematic-B* > *Nematic-A*, which correlates well with the observed decrease in ion-pair concentration. The *Nematic-A* system incorporates predominantly situations in which only one of the PEO hemi-helices in any Li–O coordination sphere is broken; as illustrated in Fig. 2. This reduces the possibilities for lower Li–O coordination, and thus leads to a higher incidence of 5-fold coordinated Li (Fig. 3). In the *Nematic-A* system, almost 50% of the ion pairs form outside the defect region, which corresponds well with the more dispersed nature of the imposed isolated defect distribution. The somewhat higher incidence of ion-pairing in the *Smectic-B vs. Nematic-B* cases is almost certainly a consequence of the more extended ordered arrangement of defects in the *smectic* case, whereby a complete defect ''layer'' is created in which ion pairs are able to form more readily.

Considering the specific role of terminal groups in promoting ion-pair formation, we see that the further the methyl-group pairs move away from their positions along the channel walls (Fig. 6c), the more they avoid one another and thereby provide more space for ion-pair formation. From Fig. 6a–c, we see that the methyl end-group separation correlates well with the incidence of ion-pair formation.

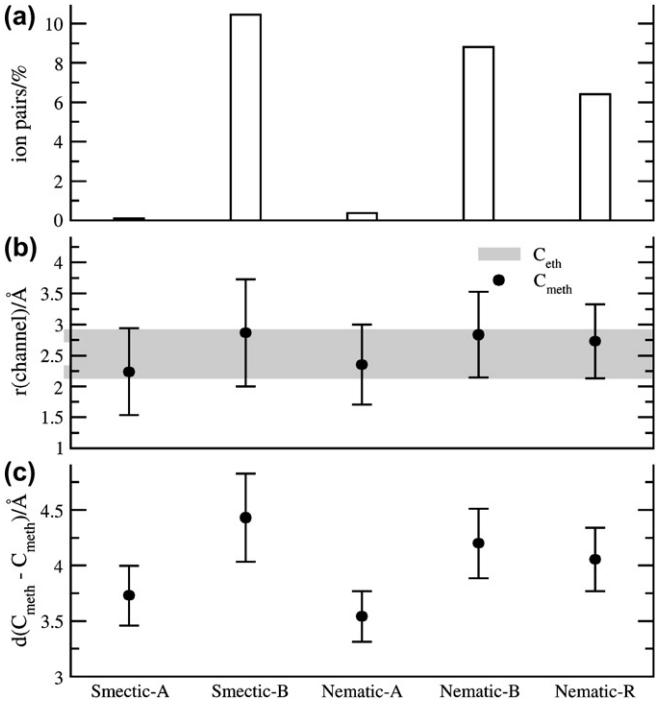

Fig. 6. (a) Percentage of Li-ions participating in ion-pairing for the five simulated models for $LiPF_6 \cdot PEO_6$ as described in Fig. 2; (b) chain-end methyl carbon (C_{meth}) displacements from the PEO channel axes compared to the displacements in defect-free PEO (C_{eth}); and (c) corresponding C_{meth}–C_{meth} separations across the chain-break regions.

3.2. The channel structure

Let us first consider how the channel structures differ in the *smectic* and *nematic* models depending on the nature of the break defect (A, B or R) (Fig. 2). The Li–Li distances are

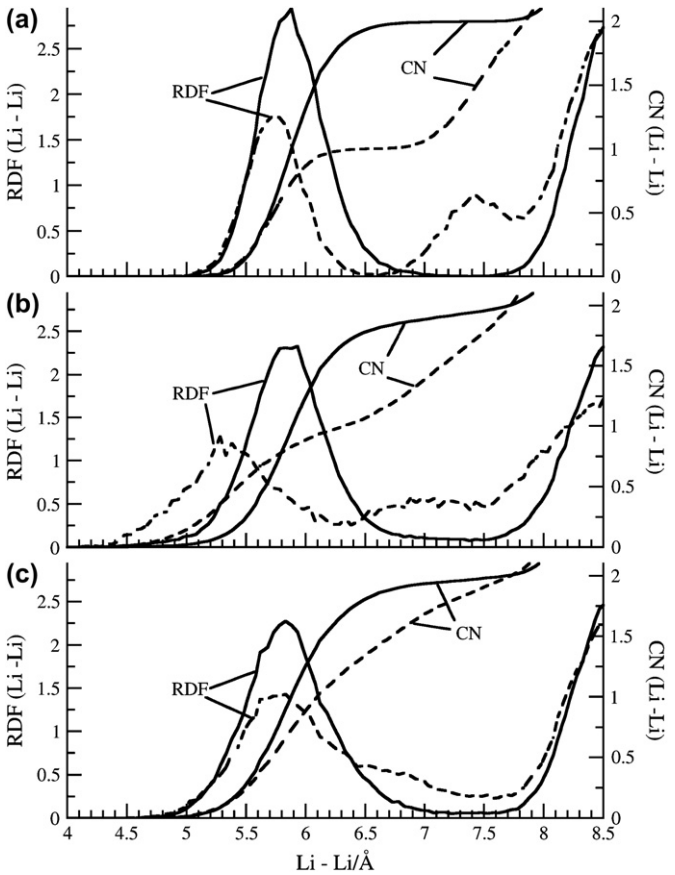

Fig. 7. Li–Li radial distribution functions RDF(Li–Li) and coordination numbers CN(Li–Li) in defect-free (solid lines) and chain defect (dashed lines) regions for different conformations of $LiPF_6 \cdot PEO_6$: (a) *Nematic-A*; (b) *Nematic-B* and (c) *Nematic-R*.

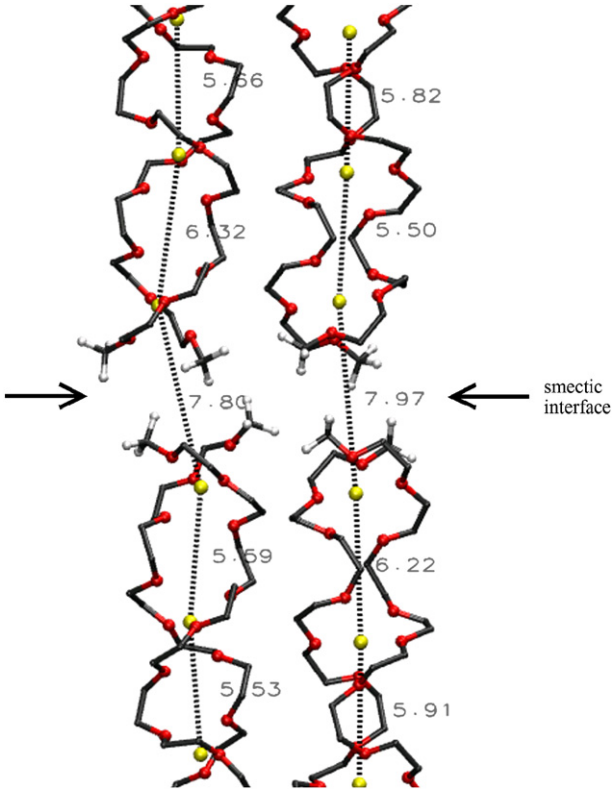

Fig. 8. Chain conformations and Li-ion coordination in the chain defect region of the *Smectic-A* model of $LiPF_6 \cdot PEO_6$; typical Li–Li distances are indicated.

found to reflect well the different structural situations for the Li-ions, especially in the chain-break regions. In the *Smectic-A* and *Nematic-A* systems, the average distance from a Li-ion in a defect region to its nearest Li neighbour is closely similar to that in a defect-free region (5.8 Å compared to 5.9 Å), while the Li–Li distance across the defect region is *ca*. 7.5 Å. This appears as an extra peak in the RDF(Li–Li) plot for the *Nematic-A* case; Fig. 7a. This peak is also present for the *Smectic-A* case (not shown), where a slight lateral displacement was noted in successive PEO channels in adjacent blocks (Fig. 8). This was also observed in our earlier study of a short-chain ($n = 23$) PEO system [9].

Li-ions in channel end defect-regions for CN(Li–O) < 6 (*i.e*., B-type systems) tend to move closer to the Li-ions in the end-regions of successive PEO channels; with Li–Li distances *ca*. 5.2 Å compared to 5.9 Å in defect-free regions (Fig. 7b). The Li–Li distances *across* the defect region vary over a broad range (6–8 Å) compared to this distance in A-type systems (Fig. 7a,b), with the shorter *ca.* 6 Å Li–Li distance corresponding to the ''chain-bridging'' configuration shown in Fig. 5. This type of local structural arrangement provides regular continuity in the Li-ion sequence across a channel break, and could therefore facilitate the experimentally observed enhanced Li-ion transport [8]. On the basis of such structural considerations, the B-type situation would therefore seem to be more likely in the real material than the A-type situation.

Chain defects in the *Nematic-R* model situation rarely involve both hemi-helices around a given Li-ion. This appears

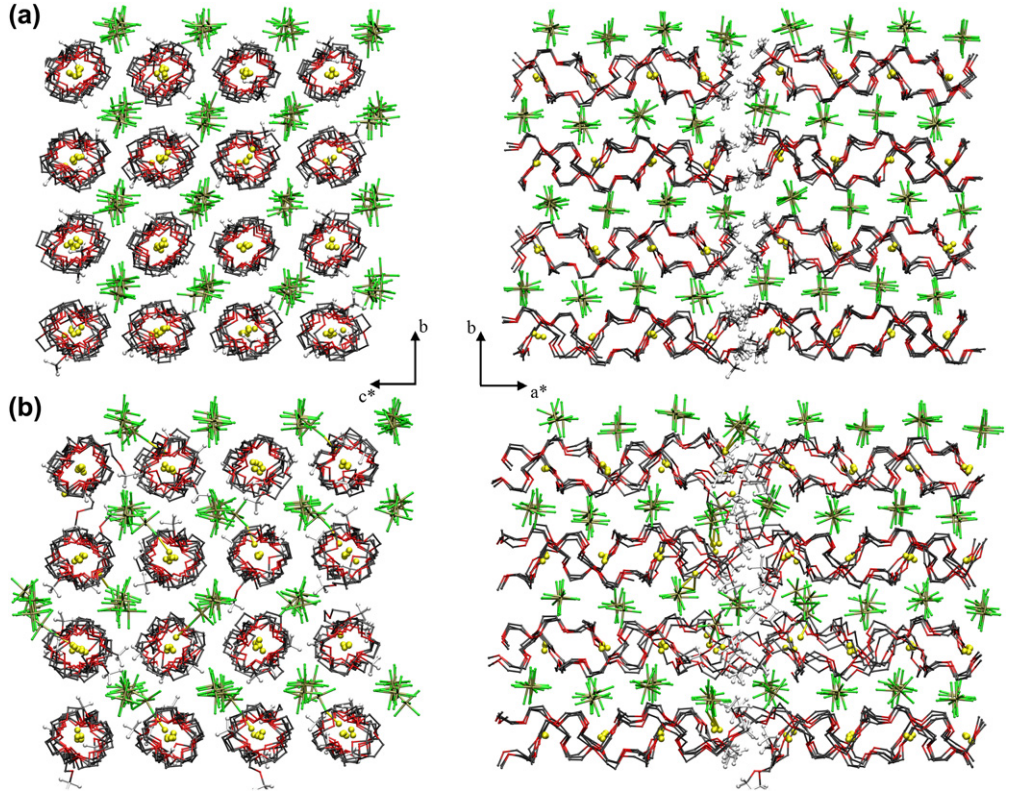

Fig. 9. MD snapshots for (a) *Smectic-A* and (b) *Smectic-B* models of short-chain $LiPF_6 \cdot PEO_6$ as viewed along the *a*- and *c*-directions.

to cause Li–Li distances in these defect regions to vary less than in the *Smectic-B* and *Nematic-B* models; typically 2 Å *vs*. 3 Å. This is also evident from the RDF(Li–Li) plots (Fig. 7a–c).

In *A-type* models involving 6-fold coordinated Li-ions, the methyl-groups also remain somewhat closer to the PEO channel axis compared to the B- and R-type situations (Fig. 6b). The shorter distance of methoxy- compared to ethoxy-carbons from the central channel axis indicates that the Li-ions in the defect regions are tightly bound to the surrounding polymers, and may well be immobilised by high activation-energy barriers to Li transport. Interestingly, even if the Li–Li distances across the gap in the *A-type* models (as discussed above) are larger than in *B-type* systems, the distance between the methyl groups across the defect are consistently shorter (Fig. 6c). This is because the methoxy groups in *B-type* systems are not coordinated to Li-ions and are therefore free to migrate away from their normal positions near the PEO channel walls into the space outside the channels (see Fig. 9).

3.3. The smectic surface

One of the prime goals of this study has been to endeavour to set up what could be best be described as *smectic* interfaces. This has been done by setting up an MD-box in which registry has been established between an array of parallel monodisperse short-chain ($n = 23$) PEO double hemi-helices, thereby creating an extended plane of methyl chain-ends at either end of ''nano-crystalline blocks''. The periodic symmetry relating the blocks generates the required *smectic* interface; see Fig. 9. Clearly, interfaces are also formed on the four sides of each block, each involving sets of parallel PEO chains. As described earlier, two types of *smectic* model (*A* and *B*) are studied, differing only in the position of the chain-breaks with respect to the Li-ions. The behaviour of the two models is found to be quite different: in the *Smectic-B* model (Fig. 9b), the PEO-tunnels link together *via* ''bridging'' methoxy groups, and the defect region involves disordered Li-ions, which could favour ion transport. In contrast, the *Smectic-A* system (Fig. 9a) exhibits neither bridging groups nor disordered Li-ions. Furthermore, the double hemi-helical PEO channels in the *Smectic-A* system show only small (~0.5 Å) lateral displacements which slightly perturb the translational symmetry of the crystallite; see Figs. 8 and 9.

3.4. Simulated XRD profiles

XRD profiles have been calculated from trajectory data from NVT simulations (Fig. 10) for each of the system simulated, using an adapted version of the DISCUS program [25]. These can be compared with the experimental XRD profile (Fig. 10: bottom figure) [26]. In this context, however, it is most important that we first consider the basis for the appearance of particularly the experimental profile. Since experimental XRD intensities (to a good approximation) only contain information regarding translational features in the unit cell structure, they will therefore not contain any direct

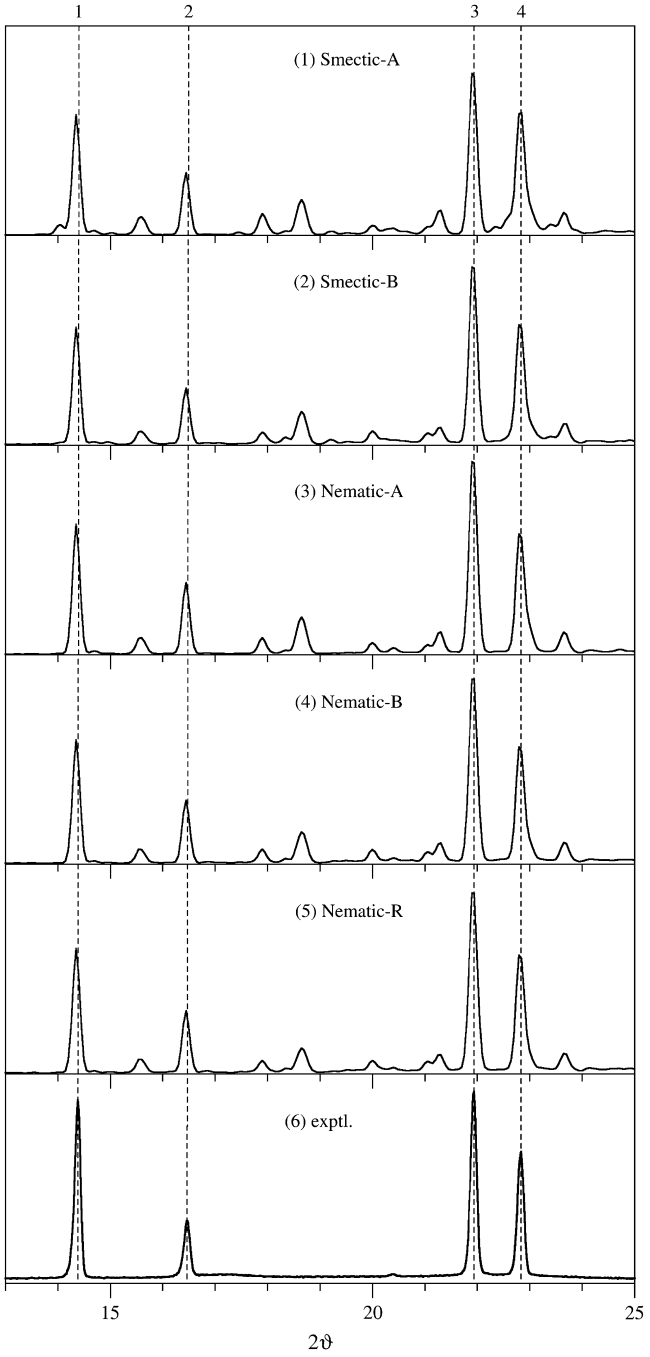

Fig. 10. Calculated XRD ''powder profiles'' for the five MD models simulated for $LiPF_6 \cdot PEO_6$ (1–5) as summarised in Fig. 2, using cell parameters constrained to values determined from the experimental XRD profile in the bottom figure. Peak widths have all been constrained to 0.16° (in 2Θ) to roughly match the experimental values.

information relating to surface or chain-end features present in the material. Two interesting situations thus arise:

- The experimental XRD data will lack information on such ''defect regions'' lying at the surfaces of the effective diffracting mosaic blocks in the real material, and refinement of the data will therefore only reflect the structure of the defect-free regions inside these blocks. This is the situation for a *smectic* arrangement; or

- When these ''defect regions'' are more or less randomly distributed throughout the real structure (as is the case for the various *nematic* models simulated), the XRD data will actually contain partial information on these defects, and refinement of the resulting XRD data will include an ''averaged-in'' weighted component of the defect regions superposed on the defect-free structure. In other words, the resulting refined model will fit less well to the data– but will, in this case, actually include the averaged-in effect of the defect distribution.

We are left therefore with the paradoxical situation that a better fit with experimental data could imply a *smectic* situation but would actually tell us little about the end-chain defects in the system, whereas a poorer fit could imply a *nematic*-type structure, since the effect of defects is now present in the experimental data but not in the refined model.

In practise, however, we see no significant differences in agreement with experiment for the *smectic* and *nematic* models. There are, however, added complications, *e.g.*, there is no direct correspondence between MD-box dimensions and the size of the scattering ''mosaic blocks''; nor have we considered the coherence length of the diffraction process itself in relation to the size of the MD-box or the ''mosaic blocks''. In short, XRD is an inappropriately crude and uncertain technique for distinguishing between possible short-chain ordering models.

4. Conclusions

The effect of different imposed distributions of methoxy chain-ends in short-chain crystalline monodisperse $LiPF_6 \cdot PEO_6$ has been studied using the MD technique. Two *smectic* and three *nematic* models have been simulated for different types of order in the chain-end registry. Rather than attempting here to identify the ''correct'' local structure, in view of the almost total lack of Li-ion mobility in the simulations in the absence of an electric field, it is more realistic to draw upon the somewhat fragmentary evidence available from the simulation of each of the five different models investigated, and endeavour to piece together some picture of the nature of the disorder in the material. Indeed, it is most unlikely that any genuinely ''correct'' structure exists – for two prime reasons:

- The low Li-ion mobility implies the probable superposition of many different metastable local structures. Our MD timescale does not yet permit us to probe such phenomena.
- The inherent inadequacy of the XRD technique to provide definitive structural information regarding order/disorder in the system (see above).

Nevertheless, two interesting features emerge from our simulations:

- The *Nematic-R*, *Nematic-B* and *Smectic-B* models all provide a structural basis for continuous transport of Li-ions along discontinuous short-chain PEO molecules.
- Simulated XRD peak intensities for all models with chain-break defects in the cation coordination sphere (*Nematic-R*, *Nematic-B* and *Smectic-B*) agrees reasonably well with experimental data.

It is possible that comparative *vibrational spectroscopy* data for mono- and polydisperse systems could distinguish ion-pairing and Li–O coordination for the different models simulated. All broken Li–O coordination regions should involve a detectable number of ion pairs. Several spectroscopic studies have already addressed structural issues regarding $LiPF_6 \cdot PEO_6$ and its *iso*-structural crystal forms [27–29]; and there is some evidence to suggest ''spectroscopically free'' anions in these materials.

Our simulation work in this area continues with more extensive studies of the same types of model addressed here, but under the influence of high electric fields to induce a higher degree of ion mobility.

Acknowledgements

We would like to acknowledge the support provided for this work by the *Swedish Science Council (VR)*; and DB would like to acknowledge stipends from Wenner-Gren Foundations and The Royal Swedish Academy of Sciences. The research has also been supported by a grant from the *Estonian Science Foundation (ETF)* (Grant No. 6763), and a stipend for AL from the *Archimedes Foundation*. The excellent service provided by the *UPPMAX Supercomputing Centre* is also gratefully acknowledged.

References

[1] Tarascon JM, Armand M. Nature 2001;414:359.
[2] van Schalwijk W, Scrosati B. Advances in lithium-ion batteries. New York: Kluwer Academic/Plenum Publishers; 2002.
[3] MacGlashan GS, Andreev YG, Bruce PG. Nature 1999;398:792.
[4] Gadjourova Z, Martin y Marero D, Andersen KH, Andreev YG, Bruce PG. Chem Mater 2001;13:1282.
[5] Gadjourova Z, Andreev YG, Tunstall DP, Bruce PG. Nature 2001; 412:520.
[6] Zhang C, Staunton E, Andreev YG, Bruce PG. JACS 2005;127:18305.
[7] Brandell D, Liivat A, Aabloo A, Thomas JO. Chem Mater 2005;17:3673.
[8] Stoeva Z, Martin-Litas I, Staunton E, Andreev YG, Bruce PG. JACS 2003;125:4619.
[9] Brandell D, Liivat A, Kasemägi H, Aabloo A, Thomas JO. J Mater Chem 2005;15:1422.
[10] Brandell D, Liivat A, Aabloo A, Thomas JO. J Mater Chem 2005;15:4338.
[11] Staunton E, Andreev YG, Bruce PG. Faraday Discuss 2007;134:143.
[12] Neyertz S, Brown D, Thomas JO. J Chem Phys 1994;101:10064.
[13] Borodin O, Smith GD. Computational materials chemistry: methods and applications. Kluwer Academic Publishing; 2004 [chapter 2].
[14] Jaffe RL, Smith GD, Yoon DY. J Phys Chem 1993;97:12752.
[15] Borodin O, Smith GD. J Phys Chem B 2003;107:6801.
[16] Smith GD, Jaffe RL, Partridge H. J Phys Chem A 1997;101:1705.
[17] Borodin O, Smith GD, Jaffe RL. J Comput Chem 2001;22:641.
[18] Smith W, Forester T. The DL_POLY project. TCS Division. Daresbury, Warrington, WA4 4AD, UK: Daresbury Laboratory.
[19] Vouyovitch L, Brown D, Neyertz S, Gallot B. Soft Mater 2002;1:93.

[20] Henderson WA, Brooks NR, Brennessel WW, Young VG. Chem Mater 2003;15:4679.
[21] Andreev YG, Seneviratne V, Khan M, Henderson WA, Frech RE, Bruce PG. Chem Mater 2005;17:767.
[22] Henderson WA, Brooks NR, Young VG. Chem Mater 2003;15: 4685.
23] Seneviratne V, Frech R, Furneaux J, Khan M. J Phys Chem B 2004;108:8124.
[24] Henderson WA, Brooks NR, Young VG. JACS 2003;125:12098.
[25] Proffen T, Neder RB. J Appl Crystallogr 1997;30:171.
[26] Andreev YG. Private communication, 2005.
[27] Burba C, Frech R. J Phys Chem B 2005;109:15161.
[28] Grondin J, Ducasse L, Bruneel JL, Servant L, Lassègues JC. Solid State Ionics 2004;166:441.
[29] Ducasse L, Dussauze M, Grondin J, Lassègues JC, Naudin C, Servant L. Phys Chem Chem Phys 2003;5:567.